







RESEARCH ARTICLE

Near-surface hydraulic conductivity of northern hemisphere glaciers

Ian T. Stevens¹ | Tristram D.L. Irvine-Fynn¹  | Philip R. Porter²  | Joseph M. Cook³  |
Arwyn Edwards^{1,4}  | Martin Smart² | Brian J. Moorman⁵  | Andy J. Hodson^{3,6}  |
Andrew C. Mitchell¹

¹Department of Geography and Earth Sciences (and Centre for Glaciology, and Interdisciplinary Centre for Environmental Microbiology), Aberystwyth University, Aberystwyth, UK

²Geography and Environmental Science, University of Hertfordshire, Hatfield, UK

³Department of Geography, University of Sheffield, Sheffield, UK

⁴Institute of Biology Environment Rural Science (and Interdisciplinary Centre for Environmental Microbiology, and Centre for Glaciology), Aberystwyth University, Aberystwyth, UK

⁵Department of Geography, University of Calgary, Alberta, Canada

⁶UNIS, Longyearbyen, Norway

Correspondence

Tristram D.L. Irvine-Fynn, Centre for Glaciology, Department of Geography and Earth Sciences, Aberystwyth University, Aberystwyth, UK.
Email: tdi@aber.ac.uk

Funding information

Aberystwyth University (Department of Geography and Earth Sciences); Gilchrist Educational Trust, Grant/Award Number: ASPECT Expedition; Climate Change Consortium for Wales, Grant/Award Number: C3W Proof of Concept; EU F7 INTERACT, Grant/Award Number: SCARFACE; Higher Education Funding Council for Wales (HEFCW), Grant/Award Number: Capital Infrastructure - Extreme Experiments Laboratory (Ex2EL); Natural Environment Research Council (NERC), Grant/Award Number: NE/M021025/1; Natural Sciences and Engineering Research Council of Canada (NSERC); Polar Continental Shelf Project (PCSP); Parks Canada; Northern Scientific Training Program (NSTP); Rolex Awards for Enterprise; Royal Geographical Society, Grant/Award Number: Postgraduate Research; Royal Society, Grant/Award Number: RG130314; Scottish Arctic Club, Grant/Award Number: ASPECT Expedition; Welsh Government and HEFCW, Grant/Award Number: Sêr Cymru National Research Network (NRN) - Low Carbon, Energy and the Environment

Abstract

The hydrology of near-surface glacier ice remains a neglected aspect of glacier hydrology despite its role in modulating meltwater delivery to downstream environments. To elucidate the hydrological characteristics of this near-surface glacial weathering crust, we describe the design and operation of a capacitance-based piezometer that enables rapid, economical deployment across multiple sites and provides an accurate, high-resolution record of near-surface water-level fluctuations. Piezometers were employed at 10 northern hemisphere glaciers, and through the application of standard bail–recharge techniques, we derive hydraulic conductivity (K) values from 0.003 to 3.519 m day^{−1}, with a mean of 0.185 ± 0.019 m day^{−1}. These results are comparable to those obtained in other discrete studies of glacier near-surface ice, and for firn, and indicate that the weathering crust represents a hydrologically inefficient aquifer. Hydraulic conductivity correlated positively with water table height but negatively with altitude and cumulative short-wave radiation since the last synoptic period of either negative air temperatures or turbulent energy flux dominance. The large range of K observed suggests complex interactions between meteorological influences and differences arising from variability in ice structure and crystallography. Our data demonstrate a greater complexity of near-surface ice hydrology than hitherto appreciated and support the notion that the weathering crust can regulate the supraglacial discharge response to melt production. The conductivities reported here, coupled with typical supraglacial channel spacing, suggest that meltwater can be retained within the weathering crust for at least several days. Not only does this have implications for the accuracy of predictive meltwater run-off models, but we also argue for biogeochemical processes and transfers that are strongly conditioned by water residence time and the efficacy of the cascade of sediments, impurities, microbes, and nutrients to downstream ecosystems. Because continued atmospheric warming will incur rising snowline elevations and glacier thinning, the supraglacial hydrological system may assume greater importance in many mountainous regions, and consequently, detailing weathering crust hydraulics represents a research priority because the flow path it represents remains poorly constrained.

KEYWORDS

aquifer, bail–recharge, hydraulic conductivity, near-surface ice, piezometer, supraglacial ecosystem, turbulent energy fluxes, weathering crust

1 | INTRODUCTION

Most glacial run-off occurs during the summer melt season and typically fluctuates according to diurnal energy balance oscillations (Hock, Jansson, & Braun, 2005). It has often been assumed that the snow-free glacier surface imparts minimal delay between meltwater generation and its delivery to englacial, subglacial, and proglacial environments (e.g., Fountain & Walder, 1998). However, meltwater storage at an ablating glacier surface has been inferred from geophysical data (e.g., Irvine-Fynn, Moorman, Williams, & Walter, 2006; Moore et al., 1999) and meltwater budgets (e.g., Irvine-Fynn, 2008; Larson, 1978; Smith et al., 2017). Discrepancies in the timing and volume of modelled ablation and observed meltwater discharge have also been observed for snow-free supraglacial catchments in alpine (e.g., Munro, 2011) and ice sheet (e.g., McGrath, Colgan, Steffen, Lauffenburger, & Balog, 2011; Rennermalm et al., 2013; Smith et al., 2017) settings. Consequently, there has been a growing recognition of the glacial *weathering crust* (Müller & Keeler, 1969): the shallow (typically 0.01–2-m) layer of porous ice, which typifies ablating glacier surfaces, which has been referred to as *honeycomb* or *coral* ice (e.g., Cutler & Munro, 1996; Zeng et al., 1984). Despite the recent surge in interest in supraglacial hydrology evident in the literature (e.g., Gleason et al., 2016; Karlstrom, Gajjar, & Manga, 2013; Karlstrom, Zok, & Manga, 2014; Mantelli, Camporeale, & Ridolfi, 2015; McGrath et al., 2011; Rippin, Pomfret, & King, 2015; Smith et al., 2015; Smith et al., 2017; St. Germain & Moorman, 2016; Yang, Karlstrom, Smith, & Li, 2016; Yang & Smith, 2013), a detailed understanding of the hydraulic conductivity (K) and permeability (k) of the weathering crust, and their variation in space and time, is still lacking (Cook, Hodson, & Irvine-Fynn, 2016; Irvine-Fynn, Hodson, Moorman, Vatne, & Hubbard, 2011; Karlstrom et al., 2014).

The porous weathering crust ice layer develops as a function of three primary drivers: (a) subsurface melt caused by incident solar radiation (Müller & Keeler, 1969; Munro, 1990), (b) heat flow within interstitial spaces that further contributes to declining ice crystal cohesion (Hoffman, Fountain, & Liston, 2014; Mader, 1992; Nye, 1991), and (c) kinetic energy and frictional heat transfers from water flow through interstitial flow paths (Koizumi & Naruse, 1994). The depth of the weathering crust that develops during synoptic clear-sky conditions is related to Beer's law (Cook, Hodson, & Irvine-Fynn, 2016; Oke, 1987), which defines an exponential increase in bulk ice density with depth (LaChapelle, 1959) from ~300–400 to 870–917 kg·m⁻³ over length scales between a few centimetres to several decimetres or more (Brandt & Warren, 1993; Müller & Keeler, 1969; Schuster, 2001; Shumskii, 1964). Factors controlling the depth of weathering crust development include the coefficient of extinction of incident short-wave radiation (SWR_{in}), itself governed by ice type, crystal size, impurity and air bubble content and their emergence rates, and the zenith angle, intensity, and duration of solar radiation receipt. Clear skies lead to glacier surface energy balance dominated by radiative fluxes, which promote weathering crust growth, in some cases of stagnating ice to a depth in excess of 2 m (Fountain & Walder, 1998; Larson, 1977). Reduced incident radiation (e.g., due to cloud cover) and high precipitation cause turbulent energy to dominate the glacier surface energy balance, promoting surface lowering, which reduces the thickness of the weathering crust (Müller & Keeler, 1969; Shumskii, 1964). Variations in the thickness and porosity of the weathering crust at synoptic

and seasonal timescales likely lead to temporal and spatial variability in supraglacial hydraulic permeability, conductivity, and meltwater storage potential. The dynamic properties of this near-surface porous medium likely influence meltwater transfer, modulating the lag time between *in situ* meltwater production and associated run-off signals (Karlstrom et al., 2014; Munro, 2011; Smith et al., 2017).

Hydraulic conductivities between 10^{-2} and 10^{-6} m s⁻¹ (10^3 and 10^{-2} m day⁻¹) for differing depths, sample times, and general surface topographies have previously been measured for glaciers in Alaska and Norway (Larson, 1977; Theakstone & Knudsen, 1981; Wakahama, 1978; Wakahama et al., 1973). In contrast, theoretical estimates based on assumed values for near-surface ice properties suggest a permeability of ~ 10^{-10} m² for the Llewellyn Glacier, Juneau Ice Field, Canada (Karlstrom et al., 2014), which given a water temperature of 0.1°C equates to a K -value to the order of 10^{-3} m day⁻¹. However, as Theakstone and Knudsen (1981) previously cautioned, rigorous comparisons of these types of data should not be made due to marked contrasts in geographical location, climatic setting, glacier morphology, and experimental methods. Rather, these limited observations emphasize the need to use a standardized approach to characterizing glacier surface hydraulic conductivity across a range of study areas to understand the processes controlling shallow-subsurface glacier hydrology.

In addition to controlling and modulating meltwater fluxes, the importance of weathering crust hydrology is of primary concern for understanding ice surface nutrient and sediment fluxes and supraglacial microbial ecology. Redistribution of fine supraglacial debris and dust across an ablating ice surface is commonly described (e.g., Adhikary, Nakawo, Seko, & Shakya, 2000; Bøggild, Brandt, Brown, & Warren, 2010; Hodson et al., 2007; Irvine-Fynn, Bridge, & Hodson, 2011; Oerlemans, Giesen, & van den Broeke, 2009; Porter, Vatne, Ng, & Irvine-Fynn, 2010), whereas hydrological flow paths in the glacier near surface control the export of microbes and associated nutrients to extraglacial environments (Cook, Hodson, & Irvine-Fynn, 2016; Hotelling, Hood, & Hamilton, 2017; Irvine-Fynn et al., 2012). The weathering crust is now recognized as an ecosystem in its own right (e.g., Cook, Edwards, Takeuchi, & Irvine-Fynn, 2016; Cook, Hodson, & Irvine-Fynn, 2016; Hodson et al., 2008; Irvine-Fynn & Edwards, 2014; Stibal, Šabacká, & Žárský, 2012). The hydrological characteristics of the weathering crust influence microbial activity in cryoconite (Edwards et al., 2011; Hodson et al., 2007; Stibal, Telling, et al., 2012), and the increased residence time afforded by percolation within the interstitial voids of the weathering crust affords microbiota, fine inorganic and organic particles, dissolved nutrients, and viruses opportunities for interaction and turnover in spite of the low growth rates and metabolic activities associated with cold environments (Rassner et al., 2016). Furthermore, legacy contaminant and particulate impurity transport through glacier systems (e.g., Bogdal et al., 2009; Hodson, 2014; Łokas, Zaborska, Kolicka, Różycki, & Zawierucha, 2016; Pavlova et al., 2014) and their accumulation in downstream environments (e.g., Bettinetti, Quadroni, Boggio, & Galassi, 2016; Bizzotto, Villa, Vaj, & Vighi, 2009; Bogdal et al., 2010) must be influenced by hydrological flow through the porous near-surface ice—a process that remains a contemporary research imperative (Grannas et al., 2013). For these reasons, with recognition of understanding, the hydraulic conductivity of the weathering crust assumes significance in the hydrology, biogeochemistry, ecotoxicology, and ecology of supraglacial systems.

To address the critical research gap weathering crust hydrological characteristics represent, we undertook the first multisite study to assess hydraulic conductivity using a consistent methodology adapted from terrestrial hydrology. Traditional techniques developed for groundwater investigations can be applied to glacial environments (e.g., Derikx, 1973; Sharp, Richards, & Tranter, 1998). Soil and bedrock aquifers are porous media with a depth-limited storage capacity, making their measurement techniques transferable to the analogous supraglacial weathering crust (cf. Hodgkins, 1997; Irvine-Fynn & Edwards, 2014; Lliboutry, 1996; Nye, 1991). A novel electronic piezometer was used to monitor water levels and recharge rates in auger holes at high temporal resolution to derive hydraulic conductivity (K) values. We describe the findings from eight valley glaciers distributed across the Northern Hemisphere, and two sites at the western margin of the Greenland Ice Sheet, and elucidate potential drivers of weathering crust development and hydraulic properties.

2 | MATERIALS AND METHODS

To examine the hydraulic conductivity, K , of the glacial weathering crust, we employed piezometer-based techniques adapted from those used to measure groundwater transfers (Amoozegar & Warrick, 1986; Freeze & Cherry, 1979). Recently, a similar approach has been used to examine the firm aquifer on the Greenland Ice Sheet (see Miller et al., 2017).

2.1 | Electronic piezometer design

Capacitance piezometers have been well described in the literature (e.g., Baxter, 1997; Reverter, Li, & Meijer, 2007; Ross, 1983; Wilner, 1960). Here, a complementary metal-oxide semiconductor device (e.g., Texas Instruments; item TLC555CP) was configured in a circuit that acts as an oscillator with an output frequency determined by the capacitance of capacitor C1 and the resistance of resistor R2 (Figure 1a,c). The capacitor was created using a 0.6 m length of 50 mm polypropylene tubing inside which was placed a 50-cm length of 1-mm aluminium angle and a looped 0.25 mm (30 AWG) Kynar insulated silver-plated copper wire (Figure 1b). The Kynar wire is kept taut by anchoring the wire with a 3 mm nylon bolt at the top of the aluminium angle, with a 25 mm × 4 mm stainless steel extension spring secured with a nylon bolt at the base of the aluminium angle (see also Ross, 1983). Regular holes are drilled around the circumference of the tube along its length, to allow uninterrupted ingress and egress of water. The frequency of the output signal scales in proportion to capacitance; as the water level rises, capacitance is reduced, output frequency increases, and vice versa. To reduce heat transfer between the device and ice surface, tubes are coated in adhesive silver foil. This foil cover was found to reduce the exposed tube temperatures by 0.5 °C when subjected to typical mountain environment conditions. The addition of a frequency to voltage convertor (e.g., Texas Instruments, LM2907N) produces a single-ended voltage output of between 1.0 and 2.8 V, which, here, is logged using a self-powered USB Track-it Data Logger (Monarch Instruments). The circuitry and battery are housed at the top of the piezometer within the plastic tube and require minimal weatherproofing. The design of the circuit means that output frequency is independent of supply voltage; therefore, there is

negligible variation to the output signal due to battery depletion, making the sensors well suited to deployment in remote environments where regular battery changes may not be possible. Piezometer output is close to linear and is not influenced by electrical conductivity, suspended sediment concentration, or temperature levels within the limits commonly observed in supraglacial environments (Figure 1d–f). Calibration of individual piezometers is simply a matter of recording voltage at a variety of known, incremental water levels and applying a linear function to the resultant datasets.

2.2 | Electronic piezometers: data processing

Aquifer hydraulic conductivity (K) is commonly assessed using piezometer tests, which quantify the nature of hydrological recovery of an auger hole following a disturbance to the water level, where auger holes are either emptied (bail test) or artificially overfilled (slug test) (Amoozegar & Warrick, 1986; Freeze & Cherry, 1979; Moore, 2002). A notable issue with the application of slug testing in the glacial environment is caused by the low permeability (e.g., Lliboutry, 1971; Lliboutry, 1996; Nye, 1991) and density gradient (e.g., Müller & Keeler, 1969) of ice when compared with a soil aquifer for which the test was designed. By introducing additional water to an auger hole, the water table would artificially rise and water would flow through the unsaturated, higher porosity weathering crust and likely result in an overestimation of *in situ* K . The bail-recharge method was considered more appropriate for use in the supraglacial environment, although water flow into the auger hole occurs isotropically from three dimensions as a false water head is generated by the empty hole (Figure 2; Moore, 2002). However, by considering the rate of water level rise, this phenomenon can be eliminated mathematically with several solutions proposed, including the formulation by Bouwer and Rice (1976):

$$K = \frac{Q \cdot \ln\left(\frac{R_e}{r_w}\right)}{2\pi \cdot L \cdot y} \quad (1)$$

where Q is the water flow into the auger hole ($\text{cm}^3 \text{ s}^{-1}$) and the remaining length terms (all in centimetres) include L , the height of the well through which water enters; y , the vertical distance between the water surface in the auger hole and the equilibrium water table; R_e , the effective radius over which y is dissipated, and r_w , the radius of the auger hole. For the equation to be valid, a single auger hole is required, and it is specifically applicable to partially penetrating, unsealed wells in unconfined aquifers, such as the weathering crust. Q can be defined through knowledge of the auger hole dimensions and the recharge rate detailed in the output from the piezometer as the water level recovers. Although R_e can be determined empirically using axisymmetric node networks (Bouwer & Rice, 1976), the term $\ln(R_e/r_w)$ can be determined using an approximation given as:

$$\ln\left(\frac{R_e}{r_w}\right) = \left[\frac{1.1}{\ln\left(\frac{h}{r_w}\right)} + \frac{A + B \cdot \ln[(D-h)/r_w]}{L/r_w} \right]^{-1} \quad (2)$$

for which D is the distance between the water table in the aquifer and the impermeable ice representing the base of the aquifer and h the depth of the water in the auger hole (both in centimetres). A and B are dimensionless constants, determined using the ratio L/r_w (see

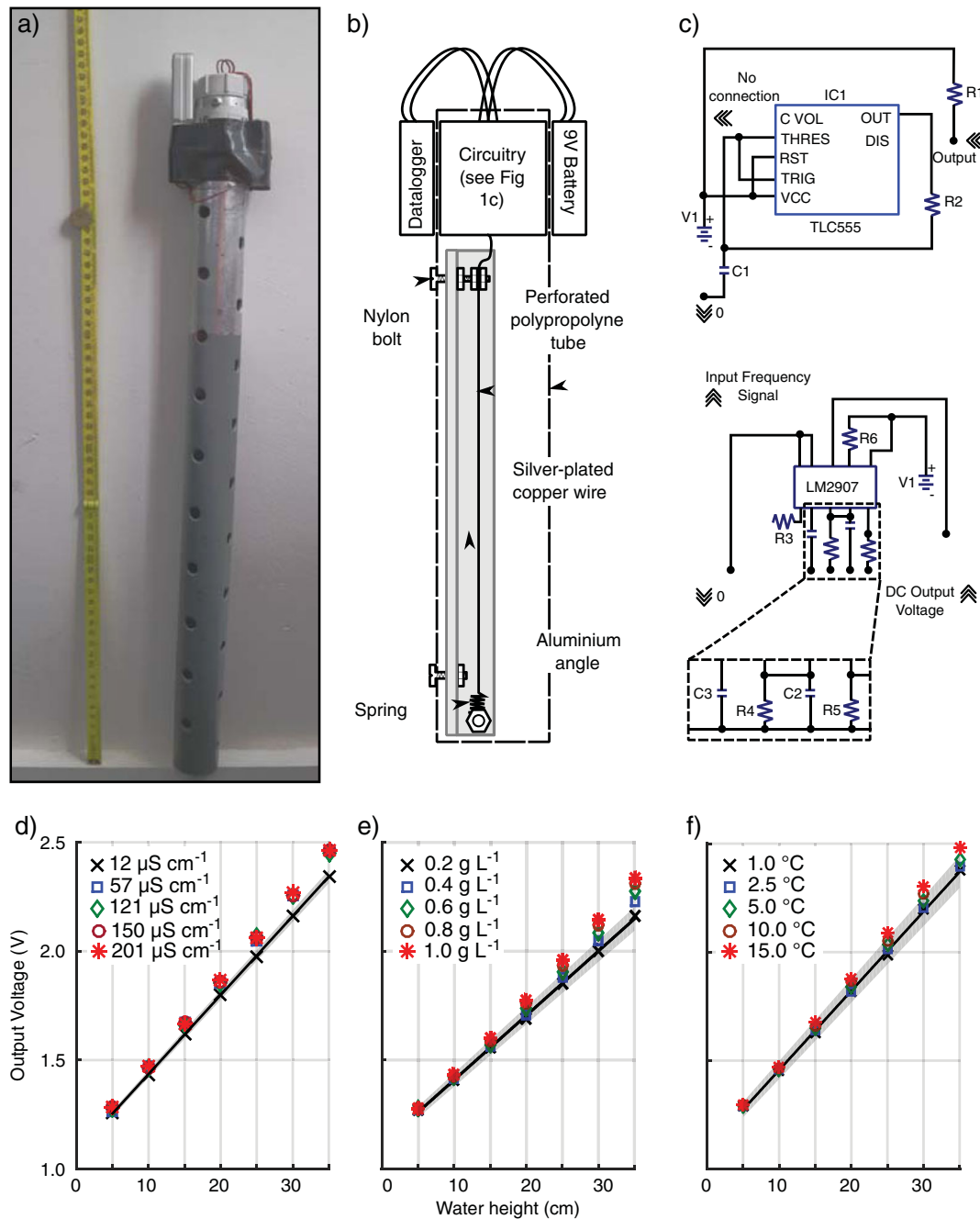


FIGURE 1 Probe design and calibration: (a) image of a water-level probe including a centimetre scale; (b) cartoon schematic of the probe design; and (c) wiring diagram for the probe circuitry. Probe voltage outputs at given water levels under specific water load conditions, for the typical supraglacial conditions (x) and for other variable conditions of electrical conductivity (d), suspended sediment load (e), and temperature (f), with the black line indicating a linear regression ($r^2 > 0.99$) and the greyed area reflecting the 95% confidence bound

Bouwer & Rice, 1976). One condition of the empirical approximation presented in Equation 2 is that $0 < (D - h)/r_w \leq 6$; if these conditions are not met, $(D - h)/r_w$ is adjusted to equal 6.

Following the derivation of K , primary ice permeability (κ) can be calculated, after Bear (1972):

$$\kappa = K \frac{\mu}{\rho_w g} \quad (3)$$

where ρ_w is the density of water (taken as $1,000 \text{ kg m}^{-3}$), g is acceleration due to gravity (0.981 m s^{-2}), and μ is the dynamic viscosity of water (in Pa s). Water viscosity is temperature dependent (Figure 3), and in the range of interest characteristic for supraglacial water

temperatures ($< 2^{\circ}\text{C}$; Isenko, Naruse, & Mavlyudov, 2005), it is useful to note that viscosities are 1.4 to 1.8 times that at 20°C .

2.3 | Hydrological data collection

Bail-recharge tests were conducted at 10 sites across the northern hemisphere cryosphere, bridging a range of latitudes and climatic settings (Table 1; Figure 4). At Haut Glacier d'Arolla, Switzerland, and Fountain Glacier Bylot Island (HACH and FGBI, respectively), holes were drilled at strategic locations along transects or semi-randomized grids within a defined supraglacial microcatchment, whereas on the K-transect of western Greenland (GRDS), nine holes were distributed

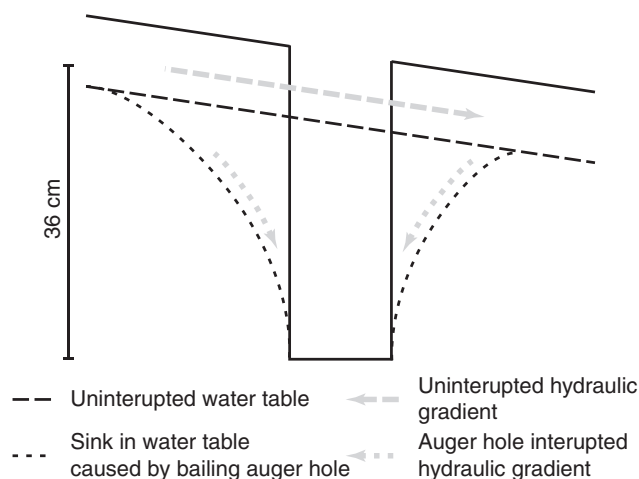


FIGURE 2 The role of auger hole drilling on the water table and idealized hydraulic head. The drilling and bailing of an auger hole causes a localized drop in the water table (with radius up to 2 m) altering the hydraulic gradient. Note that the hydraulic gradient indicated corresponds with the water table of the same line style

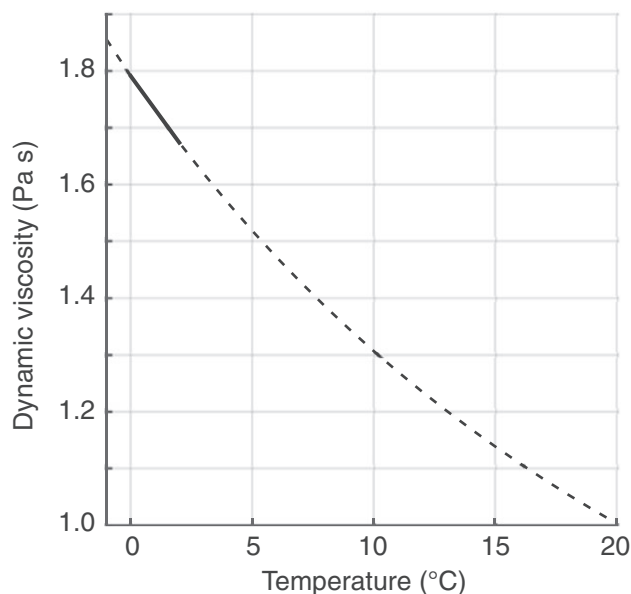


FIGURE 3 Dynamic viscosity, μ , of water as controlled by temperature in the range $-1\text{ }^{\circ}\text{C} \geq t \geq 20\text{ }^{\circ}\text{C}$ (after Kestin, Sokolov, & Wakeham, 1978). Note that the area of interest, $0.1\text{ }^{\circ}\text{C} \geq t \geq 2\text{ }^{\circ}\text{C}$, aligning with observed auger hole temperatures, is highlighted with a solid line

across a $30 \times 30\text{ m}$ grid. At other sites including those in Sweden (SGSE and RGSE), in Austria (RMOS and GBOS), at the Greenland Ice Sheet margin (GRKM), and in Svalbard (PBSV and FFSV), experiments were conducted opportunistically using glacier-wide randomized grid sampling or short transects over smaller, hydrologically active areas.

At all sites, 36 cm deep auger holes were drilled using a 5 cm diameter Kovacs drill. The auger hole depth enabled the upper 30 cm of the weathering crust to be examined, as there is a 6 cm dead space at the base of the piezometer. Auger holes were emptied using a biOrb™ manual syphon with a 5 cm nozzle head. The piezometer was inserted immediately, and recharge monitored at 2 s intervals. In cases where auger holes were reused during a single day, ablation resulted in some widening of the

uppermost 5 cm of the auger hole, but this had negligible influence upon the bail-recharge experiments due to the water table typically found approximately 14 cm below the glacier surface. The representativeness of the 36 cm deep auger holes is assessed in Section 3.1.

The time series of auger hole water column height were converted to recharge water volume and corrected to account for water displacement arising from piezometer installation. Recharge curves were manually examined and divided into three distinct stages (Figure 5): (a) Stage 1 is a linear stage that represents pressure-driven recharge as a result of the artificial water head generated by the presence of the bailed auger hole within the weathering crust; (b) Stage 2 is a nonlinear decreasing stage (i.e., recharge rate falls with time/rise in auger hole water level), identified as representing a reduction in the influence of pressure-driven flow from three dimensions and representing the flow of water through an undisturbed weathering crust (i.e., the idealized water table in Figure 2). Stage 3 is a linear stage with a gradient of 0, at which point water in the auger hole is equilibrated with the level of the water table in the surrounding weathering crust (Figure 5).

Hydraulic conductivity, K , was calculated using Equations 1 and 2, where recharge rate derived from Stage 2 defines Q , and the stable water level at Stage 3 substituted for y . To ensure $y \neq 0$, the Stage 3 auger hole recharge data were filtered and limited to 0.01 V below the voltage observed for the static equilibrium water table water depth. In the discrete cases where the auger hole exhibited incomplete recharge, either y was defined using a repeat or proximal measurement within 10 min of the curtailed measurement, or a mean water table depth for the specific glacier was used.

In the absence of detailed weathering crust density profiles with depth, we parameterized D (Equation 2) to be 40 cm, which ensured the ratio L/R_w equalled 14.4; consequently, following Bouwer and Rice's (1976) condition that for $7 < L/r_w < 16$, constants A and B (Equation 3) are defined as 2 and 0.25, respectively. The uncertainty related to this assumption was negligible: In cases where D exceeds 40 cm, there is no change in the estimated K , whereas if $D - h$ was reduced to the smallest possible value within the piezometer's measurement capabilities, there is an underestimation in K of only 6.5%. To quantify the uncertainties that resulted from the manual definition of Stage 2 in the recharge curve, a subsample of 25 recharge curves was selected randomly, covering all glaciers and a representative range of recharge rates. By identifying potential errors in the location of the transition between Stages 1 and 2 in this subsample, uncertainty in the calculated K was estimated as $\pm 4.8\%$ and again considered negligible.

2.4 | Ancillary data collection

Automated weather stations were installed locally at all sites apart from GBOS and RMOS. In a few cases, missing data were interpolated using data from the nearest alternative weather station. Where SWR_{in} data were unavailable, it was modelled (Irvine-Fynn et al., 2014) and a cloud cover correction applied using observations from local weather stations (see Greuell, Knap, & Smeets, 1997). Modelled data correlated well with measured values during the period for which directly measured SWR_{in} was available ($r^2 = 0.81$). With these data, cumulative energy input (MJ m^{-2}) from SWR_{in} since the last freeze event (i.e., temperature $< 0\text{ }^{\circ}\text{C}$) was calculated to explore the qualitative observations

TABLE 1 Summary of glacier sites sampled within the study

Glacier name	Country	Fieldwork period	Glacier code	Latitude (°N)	Area (km ²)	Elevation (m asl)	Daylight hours (decimal)	Max daily solar zenith (°)	Climate and thermal regime	Further reference
Protektorbrean	Svalbard, Norway	13/08/2015–17/08/2015	PBSV	78.24	7.60	5–700	24	25.2–26.5	Polar maritime cold	Hagen, Liestøl, Roland, and Jørgensen (1993); Hodson and Irvine-Fynn (unpublished data)
Foxfonna	Svalbard, Norway	08/08/2015	FFSV	78.12	3.95	675–950	24	28.0	Polar maritime cold	Hagen et al. (1993); Liestøl (1967); Rutter, Hodson, Irvine-Fynn, and Solås (2011)
Fountain Glacier	Bylot Island, Canada	08/07/2014–23/07/2014	FGBI	72.96	72.0	330–1,100	24	37.2–39.5	Polar continental; nontemperate polythermal	St. Germain and Moorman (2016); Wainstein, Moorman, and Whitehead, (2014); Whitehead, Moorman, and Hugenholtz (2013); Whitehead, Moorman, and Wainstein, (2014)
Rabots Glaciär	Sweden	22/08/2014	RGSE	67.91	3.70	1,070–1,640	16.4	33.8	Polar maritime; nontemperate polythermal	Björnsson (1981); Brugger (2007); Brugger, Refsnider, and Whitehill (2005)
Storglaciären	Sweden	24/08/2014	SGSE	67.90	3.10	1,120–1,730	16.1	33.1	Polar maritime; nontemperate	Björnsson (1981); Brugger (2007); Hock and Holmgren (2005); Holmlund and Eriksson (1989); Jansson (1995)
Greenland Ice Sheet (Point 660)	Greenland	06/08/2014–07/08/2014	GRKM	67.16	N/A	~630	18.2–18.3	39.6–39.9	Polar maritime; nontemperate	Smith et al. (2015); van de Wal et al. (2008); van de Wal, Greuell, van den Broeke, Reijmer, and Oerlemans (2005); Yang et al. (2016)
Greenland Ice Sheet (S6)	Greenland	22/07/2014–29/07/2014	GRDS	67.08	N/A	~1100	19.5–20.6	41.9–43.4	Polar maritime; nontemperate	
Gaisbergferner	Austria	08/09/2014	GBOS	46.83	1.03	2,460–3,390	12.9	48.8	Alpine continental; temperate	Abermann, Lambrecht, Fischer, and Kuhn (2009); Fischer (2010)
Rotmoosferner	Austria	11/09/2014	RMOS	46.82	3.17	2,450–3,000	12.9	47.6	Alpine continental; temperate	Abermann et al. (2009); Anesio et al. (2010); Edwards et al. (2013)
Haut Glacier d'Arolla	Switzerland	19/07/2015–28/07/2015	HACH	45.98	6.30	2,550–3,500	14.9–15.3	63.0–64.5	Alpine; temperate	Brock, Willis, and Sharp (2000); Mitchell, Brown, and Fuge (2001); Pellicciotti et al. (2005); Willis, Arnold, and Brock (2002)

Note. Daylight hours and solar zenith ranges are reported for the fieldwork period.

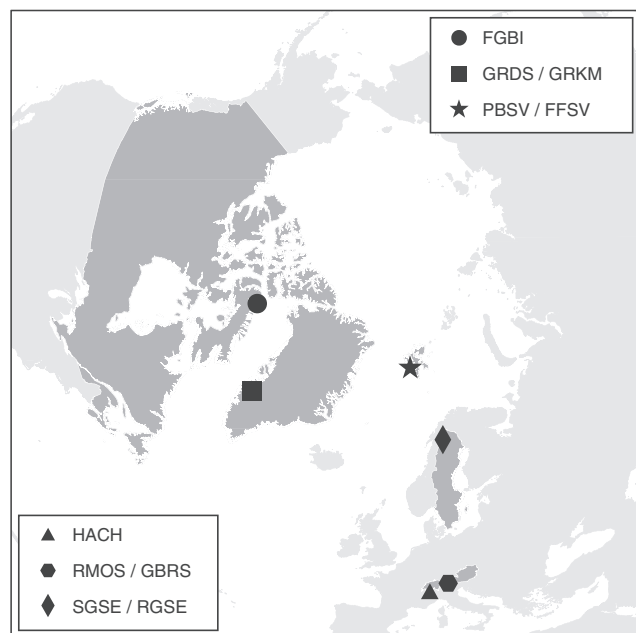


FIGURE 4 A hemispheric location map of glaciers sampled within this study. Letter codes are identified within Table 1

of Müller and Keeler (1969) regarding weathering crust development processes. For glaciers with full meteorological data, meltwater production (M) was modelled using a point-based energy balance model (Brock & Arnold, 2000) at all auger hole sites for each glacier, with a modification applied to arctic glaciers to account for the high solar azimuth (Irvine-Fynn et al., 2014).

3 | RESULTS

3.1 | Piezometer evaluation

First, to assess the representativeness of the 36 cm auger holes, comparisons were made with proximate holes with depths of 16 and

26 cm at FGBI and GRDS, with additional 46 cm deep auger holes at the former site (Figure 6). Auger holes were located within ~ 0.5 m of each other over a visually similar ice type, to minimize the influence of hole-to-hole disturbance and mitigate spatial variations in ice structure. Shapiro–Wilk tests highlighted the hydraulic conductivity data were not normally distributed at either site. For FGBI, an independent-samples median test highlighted no significant difference in median values of K between different hole depths ($p < 0.05$). However, a Kruskal–Wallis test indicated a difference in distribution of K -values across the four contrasting auger hole depth groups ($p < 0.05$), with the bounds of total ranges and interquartile ranges decreasing with an increase in auger hole depth. Dunn's post hoc testing indicated that only the 46 and 16 cm groups were significantly differently distributed from each other ($p < 0.05$). Similarly, for GRDS, an independent-samples median test indicated that median K was significantly different between the three groups ($p < 0.05$). A Kruskal–Wallis test indicated that distribution of K across the three depth groups was significantly different ($p < 0.05$), with Dunn's post hoc testing indicating the presence of a pairwise significant difference in data distribution only between the 26 and 36 cm groups ($p < 0.05$). However, there is no significant difference between any of the depth groups and the overall median for GRDS.

As there is no systematic significant difference between median K -values for auger holes of 16, 26, 36, and 46 cm in depth, any of these depths could have likely been selected as a methodological optimum. A shallow hole would require a smaller volume of water to fill and would enable a greater frequency of measurements to be recorded in a fixed period and may increase clarity of temporal trends, especially over a diurnal timescale. However, when the water table is low, shallow holes may be unsuitable as they may be perched above the water table, resulting in an inability to assess hydraulic conductivity. Conversely, a deeper auger hole (e.g., 46 cm) would be unlikely to have such an issue but would take longer to fill, reducing the frequency of K measurements. As such, we recommend and adopted 36 cm as an optimum auger hole depth as a compromise to maximize the frequency of data collection for assessment of weathering crust hydraulic parameters.

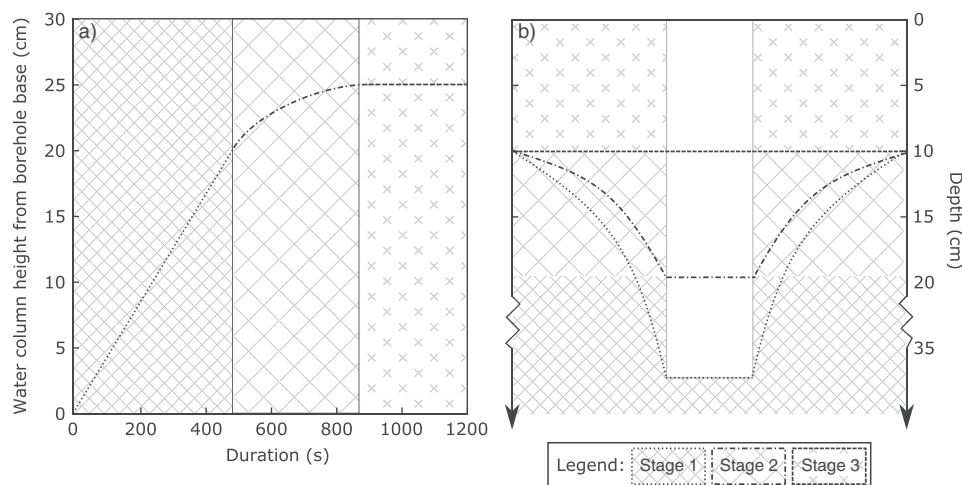


FIGURE 5 (a) An idealized recharge curve related to a schematic cross section (b) of the auger hole. In (b) each dashed line indicates the position of an idealized water table. During Stage 1, anisotropic, pressure-driven flow dominates due to the large hydraulic head generated by the presence of an auger-hole-generated (in black) sink in the water table. Through Stage 2, this influence is reduced (although still prevalent), but the influence of this false water head decreases as the hole fills (aligning with the nonlinear stage in Panel a). At Stage 3, the water level in the borehole is equilibrated with the surrounding water table and recharge stops as the auger hole becomes equilibrated with the surrounding weathering crust water table

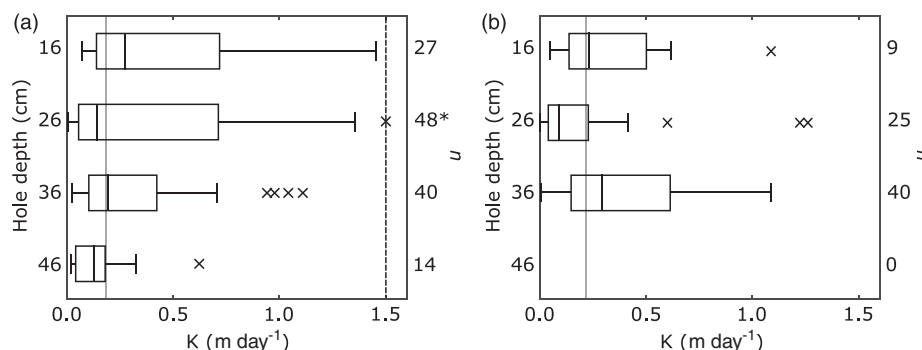


FIGURE 6 Change in K with auger hole depth for (a) FGBI and (b) GRDS, indicating median for each site (solid vertical line) of 0.183 and 0.220 m day^{-1} , respectively. Sample sizes (n) are noted on the right of the diagram. *Note one outlying data point $>1.5 \text{ m day}^{-1}$

To ascertain the repeatability of the bail–recharge method, rapid ($<15 \text{ min}$) repeat measurements were undertaken at four sites (PBSV, SGSE, GRKM, and GRDS). All repeat measurements were recorded within a maximum 30 min window to minimize any temporal variations in K . During these repeats, a constant equilibrium water table depth was assumed (range within $\pm 5\%$ of the mean) to prevent the undesirable influence of a falling water table due to aquifer drainage upon K . Relative standard deviation ($n = 19$) across the four sites was 40.9%. Of note, the contrast in medians reported for varied auger hole depths also all fell within this error associated with repeatability. Although this may appear initially to represent a high level of uncertainty in our estimates of K , typical ranges of K in groundwater studies cover a range of 13 magnitudes (Freeze & Cherry, 1979), and quantification of K to within one order of magnitude is usually sufficiently precise for most analyses (Younger, 2009). Our calculated relative standard deviation falls within this acceptable range, and as such, we are confident that our single-measure method provided suitably reliable and precise estimates of K within the weathering crust.

3.2 | Quantification of and controls upon K

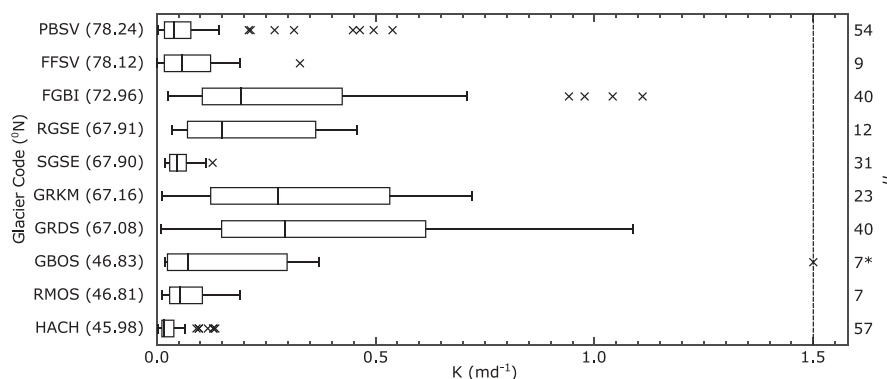
A total of 280 successful recharge experiments were conducted on 10 northern hemisphere glacier ablation zones. Twenty-five unsuccessful experiments were reported in which holes were not refilled to $>6 \text{ cm}$ depth; these were typically associated with cloudy and/or rainy conditions but had no clearly systematic cause and occurred apparently randomly across all glacier sites. Mean K across the eight field sites was $0.185 \pm 0.019 \text{ m day}^{-1}$ ($\sigma = 0.310 \text{ m day}^{-1}$, range = $0.003\text{--}3.519 \text{ m day}^{-1}$). Mean permeability was $0.384 \pm 0.060 \text{ m}^2$ (with a range

from $0.018\text{--}3.451 \text{ m day}^{-1}$). Neither hydraulic conductivity nor permeability data were normally distributed (Shapiro–Wilk, $n = 280$ and 111 , respectively, $p < 0.05$). Ranges and medians of K at each glacier plotted with site latitude as a variable (Figure 7) highlighted a potential relationship between latitude and K : A statistically significant, weak positive correlation existed between the variables (Spearman's $r = 0.140$, $p < 0.05$, $n = 280$).

To interrogate the environmental factors that may define K , specifically examining differing stages of weathering crust development, further nonparametric correlations were undertaken between K and potential explanatory variables. Such variables included water table height, as measured from the base of the 36-cm auger holes according to the Stage 3 piezometer recharge records. The potential for the water table to be influenced by the melt rate and ingress of surface water into the weathering crust was further considered by using site altitude and the energy balance model melt output (M) for the 1 hr time period preceding the observation of K as explanatory variables. Further, on the basis of Muller and Keeler's (1969) conceptual model of weathering crust development, cumulative SWR_{in} receipt since (a) freezing, (b) the previous rainfall event, and (c) the period of dominant turbulent fluxes was calculated as variables.

Freezing of interstitial meltwater may reduce interstitial pore size and decrease the hydraulic conductivity of the weathering crust. However, given the latent heat released during the refreezing of interstitial meltwater (see Paterson, 1994), a period of freezing air temperature for hours or even days is unlikely to result in complete refreezing of the liquid component of the weathering crust. However, it is important to note that such a cold wave propagates downwards (Irvine-Fynn, Hodson, et al., 2011; Paterson, 1994), so any refreezing will occur in

FIGURE 7 Box-and-whisker plot showing hydraulic conductivity of holes of 36 cm depth across all glaciers within the sample set, with latitudes displayed in degrees north of the equator. Sample sizes (n) are noted on the right of the diagram. *Note, the x axis is limited to 1.5 m day^{-1} , with one outlying point above this limit at GBOS, with a value of 3.519 m day^{-1}



the less dense, more porous upper weathering crust and hence may have a greater influence on K than would be expected. Rainfall events and cloudy periods, where turbulent fluxes dominate the energy balance equation (see Hock, 2005), are identified as crucial for resetting of the weathering crust surface (Müller & Keeler, 1969). Observations of summer rainfall are limited within our dataset; however, we assume that precipitation, as measured at local automated weather stations, is in the form of rain either supported by *in situ* observations or as defined by air temperatures in excess of 4 °C. For the available data, two periods of rainfall were identified, one at HACH, comprising a 10 hr period of overnight rainfall (17 mm total) and another at SGSE/RGSE, where 2.4 mm of rain fell in 8 hr. Melt modelling data are used to determine the ratio of SWR_{in} : turbulent fluxes at each glacier site, with a period of dominant turbulent energy flux (DTEF) defined as when >50% of energy for melt is supplied by turbulent fluxes for a duration of at least 3 hr. This duration is selected to ensure that the predominant weather pattern is that of a cloudy sky, rather than a low sun angle and high air temperatures, which can occur during sunrise and sunset. Available meteorological data allowed for determination of this variable at GRDS and SGSE/RGSE. For GRDS, two DTEF periods were observed, both between midnight (00:00) and 07:00 when the solar azimuth was low: Total melt during the two periods was 1.71 and 0.57 mm water equivalent. A more marked period of DTEF was observed at RGSE and SGSE, with a 37 and 39 hr DTEF period with 27.06 and 25.03 mm water equivalent of melt, respectively. With freezing, rainfall and DTEF periods being indicative of (at least partial) resetting of the weathering crust, cumulative SWR_{in} should identify the subsequent increase in near-surface ablation, the disaggregation of ice crystals, and increase in porosity and hydraulic conductivity.

The following significant ($p < 0.01$) monotonic correlations are highlighted between K and the following independent variables (Table 2): (a) negative correlation with cumulative SWR_{in} since freezing; (b) strong negative correlation with cumulative SWR_{in} since previous DTEF period; (c) weakly negative correlation with altitude; and (d) strongly positive correlation with water table height.

TABLE 2 Correlation matrix highlighting monotonic relationships with hypothesized controls upon hydraulic conductivity (K) of the weathering crust

Glacier	n	Cumulative SWR_{in} 0 °C	Cum. SWR_{in} precipitation	Cum. SWR_{in} DTEF	Elevation	Water table	Melt
PBSV	54	0.398**	—	—	-0.321*	0.547**	0.520**
FFSV	9	—	—	—	—	0.786*	—
FGBI	40	0.281	—	—	0.173	0.375*	—
RGSE	12	0.272	0.272	0.272	0.203	0.835**	-0.488
SGSE	31	-0.050	-0.050	-0.050	0.428*	0.249	0.212
GRDS	40 ^a	0.209	—	-0.133 (30)	0.123	0.639**	0.225
GRKM	23	—	—	—	—	0.352	—
GBOS	7	—	—	—	-0.40	0.809*	—
RMOS	7	—	—	—	-0.378	-0.204	—
HACH	57 ^a	0.098	0.112 (19)	—	0.168	0.306*	-0.253
All	280 ^a	-0.404** (234)	0.134 (62)	-0.658** (73)	-0.256**	0.710**	-0.52 (129)

Note. Sample number, n , is indicated in brackets. Values shown are Spearman's r with significant values (two-tailed) marked.

^aWith missing cases or lacking data.

* $p < 0.05$. ** $p < 0.01$.

Similar analysis was undertaken for permeability (κ ; Table 3) for PBSV and HACH located at each extreme of the latitudinal range of field sites within this study. Mean auger hole water temperatures were 0.57 ± 0.02 and 0.17 ± 0.01 °C, with ranges of 0.20–0.90 and 0.10–0.40 °C, respectively. This yielded permeability values ranging over three orders of magnitude from 0.018 and 3.45 m². However, with auger hole water temperature data only available for two glaciers, our interpretations are limited. By estimating a mean water temperature for all other glaciers, any correlations with environmental variables would simply mirror those reported for K (see Equation 5).

4 | DISCUSSION

Ablating glacier surfaces are characterized by a porous ice weathering crust that may influence meltwater, sediment, microbial cell, and nutrient storage and transport (Edwards et al., 2011; Hodson et al., 2007; Irvine-Fynn et al., 2012; Munro, 2011; Stibal, Šabacká, et al., 2012; Stibal, Telling, et al., 2012). Here, we have presented data from a low-cost capacitance piezometer, which, to our knowledge, is the first comprehensive set of measurements across multiple glacier sites using a standardized methodology to describe K for weathering crust ice.

TABLE 3 Correlation matrix highlighting monotonic relationships with hypothesized controls upon permeability (κ) of the weathering crust

Glacier	n	Cumulative SWR_{in}	Elevation	Water table	Melt
PBSV	54	0.398**	-0.321*	0.548*	.519**
HACH	57	0.093	0.171	0.304*	-.272
All	111	-0.165	-0.291**	0.574**	.415**

Note. Values shown are Spearman's r with significant values (two-tailed) marked. Latitude is not considered as independent variables due to a lack of data.

* $p < 0.05$. ** $p < 0.01$.

4.1 | Application of piezometer and Darcian flow model to the weathering crust

The piezometer described provides high-resolution water-level data. The application of the piezometer in supraglacial environments enabled quantification of the hydraulic properties of the weathering crust and was used to test the applicability of Darcy's law to the weathering crust. Darcy's law describes diffuse water flow through a homogenous porous media and is not applicable where flow is confined to or influenced by discrete conduits (karstic flow: Moore, 2002). Karstic flow would cause the recharge curves to show irregular or abrupt step changes where water suddenly enters a conduit (e.g., Hartmann, Goldscheider, Wagener, Lange, & Weiler, 2014). This characteristic or phenomenon in the recharge curves was not observed in our data, indicating that flow through the weathering crust appears to be effectively homogenous at the synoptic scale and that Darcy's law can be applied broadly with confidence to weathering crust hydrology.

4.2 | Hydraulic conductivity of the weathering crust

At the 10 sites examined across the northern hemisphere, mean weathering crust K was $0.185 \pm 0.019 \text{ m day}^{-1}$. This value is equivalent to those reported for sandstone (10^{-1} – 10^1 m day^{-1}) or stratified clay soil (10^{-1} – 10^2 m day^{-1} ; Bear, 1972), and hence, hydrologically, the glacial weathering crust can be considered as a poor, impervious aquifer. This also compares well, albeit an order of magnitude lower, to the recent 10^0 – 10^2 m day^{-1} estimates for the hydraulic conductivity of firn on alpine glaciers (e.g., Fountain, 1989; Schneider, 1999) and the Greenland Ice Sheet (e.g., Miller et al., 2017). Our K -values are the same order of magnitude as those reported for ablating glacier ice by Cook, Hodson, and Irvine-Fynn (2016), and similar to the lower order estimates given by previous site-specific studies (e.g., Karlstrom et al., 2014; Larson, 1977; Theakstone & Knudsen, 1981; Wakahama, 1978; Wakahama et al., 1973). Our estimated ranges of weathering crust hydraulic conductivity still encompassed the values derived from Medenhall and Llewellyn Glaciers (Juneau Icefield, Alaska/British Columbia) despite the absence of such a maritime environment in the study sites reported here.

The estimates of K in the weathering crust approaching that of sandstone or clay would seem surprising, given the degrading near-surface ice surface would suggest a higher porosity and potentially an increased hydraulic conductivity. However, hydraulic permeability and conductivity are also governed by the scale of and linkage between void spaces in a porous medium (Bear, 1972). Both the angularity of ice crystals and the immobile viscous water layers that surround them (Nye, 1991) reduce the hydraulic conductivity through, by simultaneously increasing microscale flow path tortuosity and reducing permeability. Water movement in the uppermost 2 m of a glacier is typically driven upward due to the near-surface water pressure gradient (Lliboutry, 1996) that can be influenced by meteorological conditions and is complicated further by the capillary force that retains and restricts water flow (Bear, 1972), allowing flow in opposition to the gravity- and slope-driven directions. Moreover, observations of local water tables identified in open cryoconite holes suggest that the water

table is commonly several centimetres to ~30 cm below the ice surface (Bøggild et al., 2010; Cook, Edwards, et al., 2016; Cook, Hodson, & Irvine-Fynn, 2016), and so K is retrieved for depths below the most porous surface ice. Combined with the near-surface density gradient, these mechanical conditions may in part explain the low K identified for the apparently porous weathering crust. Studies conducted in the 1970s and 1980s used contrasting methods, including dyes such as ink (Wakahama et al., 1973) and fluorescein (Theakstone & Knudsen, 1981). Ink and tracer dyes such as fluorescein and rhodamine are highly dispersive within water (Smart & Laidlaw, 1977); therefore, the use of dyes may result in an overestimation of K , as the tracer will likely have dispersed through the subsurface water column rather than acting conservatively and matching the water flow rate. Theakstone and Knudsen's (1981) work focused on the quantification of meltwater flow rates through the supraglacial drainage network, and they only estimated the delay to flow caused by the weathering crust as a component of this. Despite this difference in emphasis, our upper estimates for K coincide with Theakstone and Knudsen's median estimates, whereas the difference compared to the K -value reported for Medenhall Glacier (Karlstrom et al., 2014) may simply be due to the particular environmental and climatic setting, solar radiation receipt, and synoptic progress through individual melt seasons.

One issue arising with the use of pumped wells (e.g., Larson, 1977) for the estimation of K in glaciological environments is that the technique requires the addition of water, which causes a local increase in water table height. As SWR_{in} receipt decreases with depth in the near surface (Cook, Hodson, & Irvine-Fynn, 2016; Oke, 1987), it is expected that pore size, permeability, and K will also decrease. The inverse is also true, so by introducing a false rise in the water table, K is measured through more porous ice, which is typically above the equilibrium water table and hence not necessarily describing K for the true transmission of meltwater at a given point in time and generating artificially elevated estimates of its value. To emphasize this assertion, our data show that an increase in water table height correlates with an increase in K and highlight the need to consider methods of describing hydraulic conductivity cautiously.

4.3 | Controls upon hydraulic conductivity of the weathering crust

In the weathering crust, the mechanism for pore enlargement is hypothesized as the cumulative receipt of subsurface SWR_{in} and internal melt of ice (Cook, Hodson, & Irvine-Fynn, 2016; Hoffman et al., 2014; Müller & Keeler, 1969). This is evidenced by the lower bulk density and greater intergranular pore space of the weathering crust when contrasted with unweathered glacier ice (LaChapelle, 1959; Nye, 1991). This enlargement of intercrystalline pores would result in an increase in hydraulic conductivities. The energy available for weathering crust development is constrained by latitude, typically with more intense SW_{in} and higher summer season air temperature even at elevation in lower latitudes. Latitude is weakly positively correlated with K , but Figure 7 indicates that the highest K -values are observed in the 67–72°N latitude band. This relationship is complicated by regional climatology, synoptic meteorology, and local altitude and topography (Barry, 2008). For example, summer cloud cover and

precipitation are common in both the Alps (e.g., Rudolph, Friedrich, & Germann, 2011) and High-Arctic Svalbard (e.g., Førlund & Hanssen-Bauer, 2000), and these conditions are known to reduce or minimize weathering crust development (Müller & Keeler, 1969). Shading by surrounding terrain will also affect SWR_{in} receipt and moderate the formation and evolution of a porous surface ice layer, whereas particularly in middle and high latitudes, as a consequence of solar geometry, glacier orientation and surface slope may become more influential. Sites characterized by higher katabatic wind speeds may experience elevated turbulent energy fluxes that reduce the efficacy of weathering crust development.

The analyses seeking to identify such additional potential controlling factors on K in terms of cumulative SWR_{in} receipt since any partial or complete resetting of the weathering crust resulted in less intuitive conclusions. The negative correlations between K and SWR_{in} since last freezing and DTEF periods indicated that as the weathering crust developed, there was a reduction in the hydraulic permeability. This was unexpected as low radiative and high turbulent energy transfers, such as cloudy periods, often including rainfall, have been anecdotally linked with weathering crust removal (Müller & Keeler, 1969). Consequently, such synoptic conditions were expected to be associated with lowered K , as was evident from several of the failed recharge experiments. Here, to explain the apparently inverse relationship between K and cumulative SWR_{in} , we suggest that the development and rise of a water table is not necessarily coincidental with progressive ice crystal disaggregation; the rise in the water table may lag behind the creation of intergranular void space, implying a low water table is associated with low K -values. Supporting this argument is the observation that K is not correlated solely with the melt that might be expected to increase the water table height and hence hydraulic conductivity. This implies that additional processes are occurring, which preclude any direct relationship between melt rate and K : For example, there could be refreezing at depth within the weathering crust and reduction of liquid water volume, or the low transmission rates incur delay as pore spaces are filled. Here, there may be analogies with the progress of the wetting front in a snowpack (e.g., Marsh & Woo, 1984) or infiltration to frozen soil (e.g., Gray, Toth, Zhao, Pomeroy, & Granger, 2001), but to develop this level of process understanding would require further investigation.

The additional complexity hydrology itself may impart on defining K is best evidenced by the positive relationship between K and water table height. Observations from cryoconite holes suggest there is a variable water table height within the weathering crust both at subdiurnal and synoptic timescales (e.g., Cook, Hodson, & Irvine-Fynn, 2016). These variations may arise from the bulk density increase with depth within the weathering crust or because of a changing local base level. Once the ability of the weathering crust to transport water is exceeded by the melt input, the water table will rise into the increasingly more porous near-surface ice, and the piezometer-derived K value increases. Hydraulic conductivity and hydraulic gradient may, in this scenario, also rise if the base level for the drainage pathway remains broadly the same due to the dampened response of the supraglacial stream network to peak melt (e.g., Munro, 2011; Smith et al., 2015, 2017). However, as the weathering crust is drained as melt rates and associated water inputs reduce overnight and the

supraglacial stream base level drops, the water table and pressure head fall; hence, K is reduced. Our feedback loop between meltwater input, water table height, and K would explain why K and melt do not directly correlate as a response time is required, dependant on infiltration rate, for the water table level to rise.

Our data from 10 glacier sites show that K exhibited values over a range of four magnitudes (relative standard deviation of ~180%), and even upon individual glaciers, there is a high local-scale variability (Figure 7). Although the relationships described above provide some indications of conceivable causes in the variability in K -values, there are clearly complex interactions between potential driving meteorological variables, which are problematic to disentangle without further study. However, one further aspect that influences the fabric of the weathering crust and hence the nature of the pores within is the microscale ice structure, which is difficult to characterize and quantify and is not included within this dataset. Ice structure and fabric will directly condition pore size and shape, interstitial connectedness, and tortuosity and therefore likely influence the hydraulic behaviour of the weathering crust. Ice structure and fabric can vary across a range of length scales (see Hambrey & Lawson, 2000; Hudleston, 2015). Consequently, crystal size, packing and orientation may play an important role in defining the rate and location at which water infiltrates and is transferred through the weathering crust, by controlling potential pore size, shape, and geometry once crystal boundaries are preferentially melted to form pores.

Our data highlight that the hydrological properties of the weathering crust are conditioned by an array of influential factors, ranging from the meteorological conditions and their synoptic progression prior to evaluation of K to the hydrological and structural characteristics of the near-surface ice itself. We also hypothesize that glacier ice dynamics and net ablation may have the capacity to modulate the weathering crust and its hydrological behaviour: Glaciers exhibiting higher ice emergence rates may offset the evolution of a deeper porous surface layer, and enhanced rates of ablation and run-off may lead to an abundance of rills and streams that through energy transfers and evolving topographic variability can degrade the weathering crust and slow its vertical evolution and spatial extent. Such hydrological disturbance may also be affected by glacier surface slope (e.g., Hodson et al., 2007; Mantelli et al., 2015; Rippin et al., 2015). Here, it is clear that more systematic surveys of K under constrained environmental parameters, and over extended time frames, are required to better define the primary drivers and rates of weathering crust development and its spatial and vertical extent at subcatchment to glacier scales.

4.4 | Hydrological role of the weathering crust and relevance to impurity transport

This study highlights a typically overlooked component of the supraglacial hydrological system. Near-surface glacier ice has traditionally been considered as essentially impermeable (e.g., Hodgkins, 1997) with an abrupt, almost immediate, hydrological response time (e.g., Fountain & Walder, 1998). Our data emphasize the weathering crust as a hitherto neglected yet important aspect of supraglacial hydrology. The presence of a water table at depth below the ice surface emphasizes the potential for short-term meltwater storage, retention, and

delay in run-off. We propose that as surface ice ablates during the ablation season, under clear-sky conditions, the weathering crust develops (Müller & Keeler, 1969) and meltwater is routed through this near-surface layer. As our data show, meltwater flow through the weathering crust can be relatively slow, yet supraglacial stream discharge response to peak melt typically occurs within <12 hr (Munro, 2011). The hydraulic conductivities calculated here, coupled with typical $\leq 10^1$ m channel spacing upon glacier surfaces (e.g., Karlstrom et al., 2014), imply that a parcel of meltwater could remain within the weathering crust for a minimum of 34 hr. Therefore, our observations directly support the notions of hydrological delay and water storage within the weathering crust conjectured by Munro (2011) and Smith et al. (2017).

At synoptic and diurnal timescales, we hypothesize that in response to the energy balance, additional new meltwater enters the weathering crust, causing the water table to rise, which positively influences K and either overrides or displaces old stored or retained meltwater. This type of water turnover is common for rainfall events in terrestrial environments (e.g., Brutsaert, 2005; Lu & Godt, 2013). When melt production exceeds the infiltration rate of the weathering crust or the water table rises to the surface, it would be expected that saturated sheet flow might occur over the surface; however, due to the complex nature of glacier surfaces, sheet flow is uncommon and was not observed during our observation periods, and drainage via rills and small streams evolves quickly (e.g., Mantelli et al., 2015). However, the observation of K being dependent on water table elevation suggests the hydraulic properties exhibit a gradient with depth in the near surface, which is also spatially and temporally variable. The proportions of meltwater that may be delayed at a variety of timescales in their delivery to supraglacial rill and stream networks and the subsequent modulation of channel hydrographs remain undefined.

The presence of a near-surface aquifer on ablating glacier surfaces with a low hydraulic conductivity may also have significant implications for the transfer of impurities across exposed ice and affect biogeochemical cycling. Here, we argue that on the basis of contemporary understanding, there is a need for future research to explore a range of these potential affects. Considering the characteristic and ubiquitous presence of fine inorganic dust (e.g., Oerlemans et al., 2009; Takeuchi, 2002), microbes (e.g., Hodson et al., 2008; Irvine-Fynn & Edwards 2014; Stibal, Šabacká, et al., 2012), and other particulate impurities and contaminants (e.g. Hodson, 2014) on glacier surfaces, the poor hydraulic conductivity of the weathering crust may have important implications on the transport rate of such particulates. To date, there has been no clear or detailed assessment of the rates at which impurities are transferred over ablating ice surfaces. Irvine-Fynn et al. (2012) reported inefficient transport processes through and storage of microbial cells within the near surface of arctic glaciers. Here, the low K -values reported for numerous glaciers align well with such an assertion of inefficient water transfer. However, the relationship between impurity transport and K is unlikely to be a simple linear function due to the potential of the weathering crust to act as mechanical filter, preventing transfer of particles with diameters in excess of pore sizes, or biochemical and physiochemical processes resisting or accentuating impurity transport (e.g., Dolev, Bernheim, Davies, & Braslavsky, 2017; Jepsen, Adams, & Priscu, 2006, 2010; Mader, Pettitt, Wadham, Wolff, & Parkes,

2006). Therefore, fluctuations in the water table and of varied hydraulic conductivity at diurnal or synoptic timescales, or over space, may be crucial in defining the character of impurities transported through or from a glacier's surface. Indeed, recent work has suggested that water flux and the hydraulic delivery of dissolved nutrients within meltwater to surface microbial habitats may be a crucial influence for microbial community structure and activity (e.g., Dubnick et al., 2017; Edwards et al., 2011; Hotaling et al., 2017) and control downstream ecology and characteristics (e.g., Singer et al., 2012; Wilhelm, Singer, Fasching, Battin, & Besemer, 2013). Furthermore, when combined with typical *in situ* doubling times of the water-borne cryospheric microbial communities of <60 days, and in some instances <5 days (Anesio et al., 2010), and clear evidence of their capacity to influence nutrient cycling (Scott, Hood, & Nassry, 2010), the potential for the supraglacial weathering crust as a microbial habitat (Irvine-Fynn & Edwards, 2014) merits further investigation. Specifically, the retention of mineral dust and microbes within the weathering crust holds the potential to contribute to supraglacial biogeochemical cycles. For example, increased residence time within the weathering crust permits greater interactions between dust, dilute nutrients, low-density bacterial hosts, and their viral parasites (Rassner et al., 2016). The hydraulics of the weathering crust, and the recognition of old and new meltwater, may hold potential influence on the transfer rates for solutes and dissolved organic compounds or contaminants within the glacier system. However, the *in situ* fate of supraglacial solutes, organic compounds, and contaminants during the ablation season still remains poorly characterized.

As both Grannas et al. (2013) and Hotaling et al. (2017) concluded, there remains a pressing need to better constrain the nature and variability of supraglacial hydrological flow paths, particularly to define their impact on contaminant and impurity transfer, microbial communities, and biogeochemical function for both glacier surfaces and glacier-fed ecosystems. This is particularly significant under the spectre of projected future changes to glacier and ice sheet run-off regimes (e.g., Bliss, Hock, & Radic, 2014; Franco, Fettweis, & Ericum, 2013). In many glacierized regions, atmospheric warming, rising snowlines, and expanding ablation areas may result in extensive supraglacial hydrology even as total glacier areas decline. Similarly, glacier thinning and cooling in higher latitudes (e.g., Delcourt, Liefferinge, Nola, & Pattyn, 2013; Irvine-Fynn, Hodson, et al., 2011) may also promote an increasing dominance of supraglacial hydrology. Consequently, understanding the influence that the weathering crust has on modulating supraglacial run-off and its characteristics is important to improve predictive hydrological models. This assessment of weathering crust hydrology presents a first step to better characterizing this commonly overlooked supraglacial flow path and exploring the controls that dictate spatial and temporal variation in hydraulic conductivity of near-surface glacier ice.

5 | CONCLUSIONS

We present a robust but simple piezometer probe design that permits low-cost, high-resolution, repeatable water-level monitoring. The economical nature of the piezometer design, combined with its limited power requirements, makes it ideally suited to spatially widespread

deployment in remote locations and for hydrological applications beyond those described here. We describe a field methodology that allows spatially widespread monitoring of glacier weathering crust water-level fluctuations at multiple sites. Data collected from a spatially extensive suite of field sites allow examination of weathering crust K , and we quantify a mean K of 0.185 m day^{-1} , which is an equivalent value to that seen for sandstone and firn and, therefore, leads us to regard the weathering crust as a hydrologically poor, impervious aquifer that can delay water transfer through the supraglacial hydrological system and act as a transient, multiday storage reservoir within this network. Our data show unequivocal evidence for spatially and temporally varying supraglacial storage and regulation of meltwater, as hypothesized by Munro (2011) and Smith et al. (2017). This role of the weathering crust as a regulator of meltwater egress has the potential to impact not only on meltwater discharge but also the supraglacial ecosystem, through influencing the transport and residence time of microbes, fine mineral grains, contaminants, and associated nutrients. Such impurity and biogeochemical fluxes, and their basin-scale export, have consequent impacts upon the supraglacial and downstream environments at a range of spatial and temporal scales. Our analysis demonstrates that the precise nature of the controls that drive the hydrological characteristics of the weathering crust are clearly complex and multifaceted. Although water table height clearly exerts a fundamental control on apparent hydraulic conductivity, detailed investigations of the hydrological evolution of the glacial weathering crust and the role of hyperlocal ice structure and crystallography, and the consequent impacts on near-surface sedimentary systems and ecosystems, likely represent fruitful avenues for further investigation.

ACKNOWLEDGMENTS

Financial support for this work was gratefully received from: Aberystwyth University (Department of Geography and Earth Sciences, and Grant: URF ASPECT-12104 to TDI); Gilchrist Educational Trust (Grant: ASPECT Expedition to ITS); EU F7 INTERACT (Grant: SCARFACE to TDI and AE); Royal Geographical Society (Grant: RGS-IBG Postgraduate Research Award to ITS); Royal Society (Grant: RG130314 to AE and TDI); Scottish Arctic Club (Grant: ASPECT Expedition Award to ITS); Natural Sciences and Engineering Research Council of Canada (NSERC), Polar Continental Shelf Project (PCSP), Parks Canada, Northern Scientific Training Program (NSTP) (Grants: to BJM); Climate Change Consortium for Wales (Grant: C3W Proof of Concept to TDI). ACM and AE acknowledge support from the Welsh Government and Higher Education Funding Council for Wales (HEFCW) Sêr Cymru National Research Network (NRN) for Low Carbon, Energy and the Environment Grant and HEFCW's Capital Infrastructure funding of the Extreme Experiments Laboratory (Ex2EI). JMC acknowledges the Rolex Awards for Enterprise. TDI and JMC also acknowledge Natural Environment Research Council (NERC) Consortium Grant 'Black and Bloom' (Grant: NE/M021025/1). The Dark Snow Project and Karen Cameron and Jason Box are thanked for the support in Greenland. The authors wish to thank Stephen Jennings, Ottavia Cavalli, Stephen Brough, Sarah St Germain, Michael Hambrey, and Jayne Kamintzis for invaluable assistance throughout various field campaigns. Andy Porter

provided generous guidance with regard to the electronics and drawing of the circuit diagrams in Figure 1. Dave Kelly (Aberystwyth) is thanked for refinement and construction of the piezometer probes, developing prototypes built by Stephen Norburn (Sheffield). Jon Bridge and two anonymous reviewers are thanked for insightful comments that improved earlier versions of the manuscript.

ORCID

Tristram D.L. Irvine-Fynn  <http://orcid.org/0000-0003-3157-6646>
 Philip R. Porter  <http://orcid.org/0000-0001-5618-9189>
 Joseph M. Cook  <http://orcid.org/0000-0002-9270-363X>
 Arwyn Edwards  <http://orcid.org/0000-0003-1762-8593>
 Brian J. Moorman  <http://orcid.org/0000-0001-7565-5309>
 Andy J. Hodson  <http://orcid.org/0000-0002-1255-7987>

REFERENCES

- Abermann, J., Lambrecht, A., Fischer, A., & Kuhn, M. (2009). Quantifying changes and trends in glacier area and volume in the Austrian Ötztal Alps (1969–1997–2006). *The Cryosphere*, 3, 205–215. <https://doi.org/10.5194/tc-3-205-2009>
- Adhikary, S., Nakawo, M., Seko, K., & Shakya, B. (2000). Dust influence on the melting process of glacier ice: Experimental results from Lirung Glacier, Nepal Himalayas. *IAHS Publication*, 264, 43–52.
- Amoozegar, A., & Warrick, A. W. (1986). Hydraulic conductivity of saturated soils: Field methods. In A. Klute (Ed.), *Methods of soil analysis Part I: Physical and mineralogical methods* (pp. 735–770). Fitchburg, WI: Soil Science Society of America.
- Anesio, A. M., Sattler, B., Foreman, C., Telling, J., Hodson, A., Tranter, M., & Psenner, R. (2010). Carbon fluxes through bacterial communities on glacier surfaces. *Annals of Glaciology*, 51, 32–40. <https://doi.org/10.3189/172756411795932092>
- Barry, R. G. (2008). *Mountain weather and climate* (3rd ed.). Cambridge, UK: Cambridge University Press.
- Baxter, L. K. (1997). *Capacitive sensors: Design and applications*. New York, NY: IEEE Press.
- Bear, J. (1972). *Dynamics of fluids in porous media*. London, UK: Elsevier.
- Bettinetti, R., Quadroni, S., Boggio, E., & Galassi, S. (2016). Recent DDT and PCB contamination in the sediment and biota of the Como Bay (Lake Como, Italy). *Science of the Total Environment*, 542A, 404–410. <https://doi.org/10.1016/j.scitotenv.2015.10.099>
- Bizzotto, E. C., Villa, S., Vaj, C., & Vighi, M. (2009). Comparison of glacial and non-glacial-fed streams to evaluate the loading of persistent organic pollutants through seasonal snow/ice melt. *Chemosphere*, 74(7), 924–930. <https://doi.org/10.1016/j.chemosphere.2008.10.013>
- Björnsson, H. (1981). Radio-echo sounding maps of Storglaciaren, Isfallsglaciaren and Rabots Glaciär, Northern Sweden. *Geografiska Annaler*, 63A, 225–231. <https://doi.org/10.2307/520835>
- Bliss, A., Hock, R., & Radic, V. (2014). Global response of glacier runoff to twenty-first century climate change. *Journal of Geophysical Research: Earth Surface*, 119(4), 717–730. <https://doi.org/10.1002/2013JF002931>
- Bogdal, C., Scheringer, M., Schmid, P., Bläuenstein, M., Kohler, M., & Hungerbühler, K. (2010). Levels, fluxes and time trends of persistent organic pollutants in Lake Thun, Switzerland: Combining trace analysis and multimedia modeling. *Science of the Total Environment*, 408, 3654–3663. <https://doi.org/10.1016/j.scitotenv.2010.04.038>
- Bogdal, C., Schmid, P., Zennegg, M., Anselmetti, F. S., Scheringer, M., & Hungerbühler, K. (2009). Blast from the past: Melting glaciers as a relevant source for persistent organic pollutants. *Environmental Science & Technology*, 43, 8173–8177. <https://doi.org/10.1021/es901628x>
- Bøggild, C. E., Brandt, R. E., Brown, K. J., & Warren, S. G. (2010). The ablation zone in northeast Greenland: ice types, albedos and impurities.

- Journal of Glaciology*, 56(195), 101–113. <https://doi.org/10.3189/002214310791190776>
- Bouwer, H., & Rice, R. C. (1976). A slug test determining hydraulic conductivity of unconfined aquifers with completely or partially penetrating wells. *Water Resources Research*, 12, 423–428.
- Brandt, R. E., & Warren, S. G. (1993). Solar-heating rates and temperature profiles in Antarctic snow and ice. *Journal of Glaciology*, 39, 99–110.
- Brock, B. W., & Arnold, N. S. (2000). A spreadsheet-based (Microsoft Excel) point surface energy-balance model for glacier and snow melt studies. *Earth Surface Processes and Landforms*, 25, 649–658.
- Brock, B. W., Willis, I. C., & Sharp, M. J. (2000). Measurement and parameterization of albedo variations at Haut Glacier d'Arolla, Switzerland. *Journal of Glaciology*, 46, 675–688. <https://doi.org/10.3189/172756500781832675>
- Brugger, K. A. (2007). The non-synchronous response of Rabots Glaciär and Storglaciären, northern Sweden, to recent climate change: A comparative study. *Annals of Glaciology*, 46, 275–282. <https://doi.org/10.3189/172756407782871369>
- Brugger, K. A., Refsnider, K. A., & Whitehill, M. F. (2005). Variation in glacier length and ice volume of Rabots Glaciär, Sweden, in response to climate change, 1910–2003. *Annals of Glaciology*, 42, 180–188. <https://doi.org/10.3189/172756405781813014>
- Brutsaert, W. (2005). *Hydrology: An introduction*. Cambridge University Press.
- Cook, J., Edwards, A., Takeuchi, N., & Irvine-Fynn, T. (2016). Cryoconite: The dark biological secret of the cryosphere. *Progress in Physical Geography*, 40(1), 66–111.
- Cook, J. M., Hodson, A. J., & Irvine-Fynn, T. D. L. (2016). Supraglacial weathering crust dynamics inferred from cryoconite hole hydrology. *Hydrological Processes*, 30(1), 433–446. <https://doi.org/10.1002/hyp.10602>
- Cutler, P. M., & Munro, D. S. (1996). Visible and near-infrared reflectivity during the ablation period on Peyto Glacier, Alberta, Canada. *Journal of Glaciology*, 42, 333–340.
- Delcourt, C., Liefvering, V., Nola, M., & Pattyn, F. (2013). The climate memory of an Arctic polythermal glacier. *Journal of Glaciology*, 59(218), 1084–1092. <https://doi.org/10.3189/2013JoG12J109>
- Derikx, L. (1973). Glacier discharge simulation by groundwater analogue. *IAHS Publication*, 95, 29–40.
- Dolev, M. B., Bernheim, R., Davies, P. L., & Braslavsky, I. (2017). Putting life on ice: Bacteria that bind to frozen water. *Journal of the Royal Society Interface*, 13, 20160210. <https://doi.org/10.1098/rsif.2016.0210>
- Dubnick, A., Kazemi, S., Sharp, M., Wadham, J., Hawkings, J., Beaton, A., & Lanoil, B. (2017). Hydrological controls on glacially exported microbial assemblages. *Journal of Geophysical Research: Biogeosciences*, 122(5), 1049–1061. <https://doi.org/10.1002/2016JG003685>
- Edwards, A., Anesio, A. M., Rassner, S. M., Sattler, B., Hubbard, B., Perkins, W. T., ... Griffith, G. W. (2011). Possible interactions between bacterial diversity, microbial activity and supraglacial hydrology of cryoconite holes in Svalbard. *The ISME Journal*, 5, 150–160. <https://doi.org/10.1038/ismej.2010.100>
- Edwards, A., Pachebat, J. A., Swain, M., Hegarty, M., Hodson, A. J., Irvine-Fynn, T. D. L., ... Sattler, B. (2013). A metagenomic snapshot of taxonomic and functional diversity in an alpine glacier cryoconite ecosystem. *Environmental Research Letters*, 8, 035003. <https://doi.org/10.1088/1748-9326/8/3/035003>
- Franco, B., Fettweis, X., & Erpicum, M. (2013). Future projections of the Greenland Ice Sheet energy balance driving the surface melt. *The Cryosphere*, 7, 1–18. <https://doi.org/10.5194/tc-7-1-2013>
- Fischer, A. (2010). Klima und Gletscher in Obergurgl. In E.-M. Koch, & B. Erschblamer (Eds.), *Glaziale und periglaziale Lebensräume im Raum Obergurgl. Alpine Forschungsstelle Obergurgl 1* (pp. 53–72). Innsbruck, Austria: Innsbruck University Press hdl:10013/epic.41196.d001.
- Förland, E. J., & Hanssen-Bauer, I. (2000). Increased precipitation in the Norwegian Arctic: True or false? *Climatic Change*, 46, 485–509.
- Fountain, A. G. (1989). The storage of water in, and hydraulic characteristics of, the firm of South Cascade Glacier, Washington State, USA. *Annals of Glaciology*, 13, 69–75.
- Fountain, A. G., & Walder, J. S. (1998). Water flow through temperate glaciers. *Reviews of Geophysics*, 36, 299–328.
- Freeze, R. A., & Cherry, J. A. (1979). *Groundwater*. Prentice-Hall, 604pp.
- Gleason, C. J., Smith, L. C., Chu, V. W., Legleiter, C. J., Pitcher, L. H., Overstreet, B. T., ... Yang, K. (2016). Characterizing supraglacial meltwater channel hydraulics on the Greenland Ice Sheet from in situ observations. *Earth Surface Processes and Landforms*, 41(14), 2111–2122.
- Grannas, A., Bogdal, C., Hageman, K., Halsall, C., Harner, T., Hung, H., ... Macdonald, R. (2013). The role of the global cryosphere in the fate of organic contaminants. *Atmospheric Chemistry and Physics*, 13, 3271–3305.
- Gray, D. M., Toth, B., Zhao, L., Pomeroy, J. W., & Granger, R. J. (2001). Estimating areal snowmelt infiltration into frozen soils. *Hydrological Processes*, 15(16), 3095–3111.
- Greuell, W., Knap, W. H., & Smeets, P. C. (1997). Elevational changes in meteorological variables along a midlatitude glacier during summer. *Journal of Geophysical Research—Atmospheres*, 102(D22), 25941–25954. <https://doi.org/10.1029/97JD02083>
- Hagen, J. O., Liestøl, O., Roland, E., & Jørgensen, T. (1993). *Glacier atlas of Svalbard and Jan Mayen*. Norsk Polarinstitutt: Oslo, Norway.
- Hambrey, M. J., & Lawson, W. (2000). Structural styles and deformation fields in glaciers: A review. *Geological Society, London, Special Publications*, 176(1), 59–83.
- Hartmann, A., Goldscheider, N., Wagener, T., Lange, J., & Weiler, M. (2014). Karst water resources in a changing world: Review of hydrological modeling approaches. *Reviews of Geophysics*, 52, 218–242. <https://doi.org/10.1002/2013RG000443>
- Hock, R. (2005). Glacier melt: a review of processes and their modelling. *Progress in Physical Geography*, 29(3), 362–391.
- Hock, R., & Holmgren, B. (2005). A distributed surface energy-balance model for complex topography and its application to Storglaciären, Sweden. *Journal of Glaciology*, 51, 25–36. <https://doi.org/10.3189/172756505781829566>
- Hock, R., Jansson, P., & Braun, L. N. (2005). Modelling the response of mountain glacier discharge to climate warming. In U. M. Huber, H. K. M. Bugmann, & M. A. Reasoner (Eds.), *Global change and mountain regions: An overview of current knowledge* (pp. 243–252). Dordrecht, The Netherlands: Springer Netherlands.
- Hodgkins, R. (1997). Glacier hydrology in Svalbard, Norwegian high arctic. *Quaternary Science Reviews*, 16, 957–973. [https://doi.org/10.1016/S0277-3791\(97\)00032-2](https://doi.org/10.1016/S0277-3791(97)00032-2)
- Hodson, A. J. (2014). Understanding the dynamics of black carbon and associated contaminants in glacial systems. *Wiley Interdisciplinary Reviews: Water*, 1, 141–149. <https://doi.org/10.1002/wat2.1016>
- Hodson, A. J., Anesio, A. M., Ng, F., Watson, R., Quirk, J., Irvine-Fynn, T. D. L., ... Sattler, B. (2007). A glacier respires: Quantifying the distribution and respiration CO₂ flux of cryoconite across an entire Arctic supraglacial ecosystem. *Journal of Geophysical Research*, 112(G4). <https://doi.org/10.1029/2007jg000452>
- Hodson, A., Anesio, A. M., Tranter, M., Fountain, A., Osborn, M., Prisco, J., ... Sattler, B. (2008). Glacial ecosystems. *Ecological Monographs*, 78(1), 41–67.
- Hoffman, M. J., Fountain, A. G., & Liston, G. E. (2014). Near-surface internal melting: A substantial mass loss on Antarctic Dry Valley glaciers. *Journal of Glaciology*, 60, 361–374. <https://doi.org/10.3189/2014JoG13J095>
- Holmlund, P., & Eriksson, M. (1989). The cold surface layer on Storglaciären. *Geografiska Annaler*, 71A, 241–244. <https://doi.org/10.2307/521394>
- Hotaling, S., Hood, E., & Hamilton, T. L. (2017). Microbial ecology of mountain glacier ecosystems: Biodiversity, ecological connections, and implications of a warming climate. *Environmental Microbiology*, 19(8), 2935–2948. <https://doi.org/10.1111/1462-2920.13766>

- Hudleston, P. J. (2015). Structures and fabrics in glacial ice: A review. *Journal of Structural Geology*, 81, 1–27.
- Irvine-Fynn, T. D. L. (2008). *Modelling runoff from the maritime Arctic cryosphere: Water storage and routing and Midtre Lovenbreen*. Department of Geography, University of Sheffield.
- Irvine-Fynn, T. D. L., Bridge, J. W., & Hodson, A. J. (2011). In situ quantification of supraglacial cryoconite morphodynamics using time-lapse imaging: An example from Svalbard. *Journal of Glaciology*, 57(204), 651–657.
- Irvine-Fynn, T. D. L., & Edwards, A. (2014). A frozen asset: The potential of flow cytometry in constraining the glacial biome. *Cytometry. Part A*, 85, 3–7. <https://doi.org/10.1002/cyto.a.22411>
- Irvine-Fynn, T. D. L., Edwards, A., Newton, S., Langford, H., Rassner, S. M., Telling, J., ... Hodson, A. J. (2012). Microbial cell budgets of an Arctic glacier surface quantified using flow cytometry. *Environmental Microbiology*, 14, 2998–3012. <https://doi.org/10.1111/j.1462-2920.2012.02876.x>
- Irvine-Fynn, T. D. L., Hanna, E., Barrand, N. E., Porter, P. R., Kohler, J., & Hodson, A. J. (2014). Examination of a physically based, high-resolution, distributed Arctic temperature-index melt model, on Midtre Lovenbreen, Svalbard. *Hydrological Processes*, 28, 134–149. <https://doi.org/10.1002/Hyp.9526>
- Irvine-Fynn, T. D. L., Hodson, A. J., Moorman, B. J., Vatne, G., & Hubbard, A. L. (2011). Polythermal glacier hydrology: A review. *Reviews of Geophysics*, 49(4), RG00350. <https://doi.org/10.1029/2010rg000350>
- Irvine-Fynn, T. D. L., Moorman, B. J., Williams, J. L. M., & Walter, F. S. A. (2006). Seasonal changes in ground-penetrating radar signature observed at a polythermal glacier, Bylot Island, Canada. *Earth Surface Processes and Landforms*, 31, 892–909. <https://doi.org/10.1002/esp.1299>
- Isenko, E., Naruse, R., & Mavlyudov, B. (2005). Water temperature in englacial and supraglacial channels: Change along the flow and contribution to ice melting on the channel wall. *Cold Regions Science and Technology*, 42(1), 53–62.
- Jansson, P. (1995). Water pressure and basal sliding on Storglaciären, northern Sweden. *Journal of Glaciology*, 41, 232–240. <https://doi.org/10.3198/1995JoG41-138-232-240>
- Jepsen, S. M., Adams, E. E., & Priscu, J. C. (2006). Fuel movement along grain boundaries in ice. *Cold Regions Science and Technology*, 45(3), 158–165. <https://doi.org/10.1016/j.coldregions.2006.05.005>
- Jepsen, S. M., Adams, E. E., & Priscu, J. C. (2010). Sediment melt-migration dynamics in perennial Antarctic lake ice. *Arctic, Antarctic, and Alpine Research*, 42(1), 57–66. <https://doi.org/10.1657/1938-4246-42.1.57>
- Karlstrom, L., Zok, A., & Manga, M. (2014). Near-surface permeability in a supraglacial drainage basin on the Llewellyn Glacier, Juneau Icefield, British Columbia. *The Cryosphere*, 8, 537–546. <https://doi.org/10.5194/tc-8-537-2014>
- Karlstrom, L., Gajjar, P., & Manga, M. (2013). Meander formation in supraglacial streams. *Journal of Geophysical Research—Earth Surface*, 118, 1897–1907. <https://doi.org/10.1002/jgrf.20135>
- Kestin, J., Sokolov, M., & Wakeham, W. A. (1978). Viscosity of liquid water in the range –8°C to 150°C. *Journal of Physical and Chemical Reference Data*, 7(3), 941–948.
- Koizumi, K., & Naruse, R. (1994). Experiments on formation of water channels in a glacier. *Journal of the Japanese Society of Snow and Ice*, 56, 137–144. <https://doi.org/10.5331/seppyo.56.137>
- LaChapelle, E. (1959). Errors in ablation measurements from settlement and sub-surface melting. *Journal of Glaciology*, 3, 458–467.
- Larson, G. J. (1977). *Internal drainage of stagnant ice: Burroughs Glacier, Southeast Alaska*. Institute of Polar Studies, Ohio State University.
- Larson, G. J. (1978). *Meltwater storage in a temperate glacier: Burroughs Glacier, Southeast Alaska*. Institute of Polar Studies, Ohio State University.
- Liestøl, O. (1967). *Storbreen glacier in Jotunheimen*. Norway.
- Lliboutry, L. (1971). Permeability, brine content and temperature of temperate ice. *Journal of Glaciology*, 10, 15–29.
- Lliboutry, L. (1996). Temperate ice permeability, stability of water veins and percolation of internal meltwater. *Journal of Glaciology*, 42(141), 201–211.
- Łokas, E., Zaborska, A., Kolicka, M., Różycki, M., & Zawierucha, K. (2016). Accumulation of atmospheric radionuclides and heavy metals in cryoconite holes on an Arctic glacier. *Chemosphere*, 160, 162–172. <https://doi.org/10.1016/j.chemosphere.2016.06.051>
- Lu, N., & Godt, J. W. (2013). *Hillslope hydrology and stability*. Cambridge University Press.
- Mader, H. M. (1992). Observations of the water-vein system in polycrystalline ice. *Journal of Glaciology*, 38, 333–347.
- Mader, H. M., Pettitt, M. E., Wadham, J. L., Wolff, E. W., & Parkes, R. J. (2006). Subsurface ice as a microbial habitat. *Geology*, 34(3), 169–172.
- Mantelli, E., Camporeale, C., & Ridolfi, L. (2015). Supraglacial channel inception: Modeling and processes. *Water Resources Research*, 51, 7044–7063. <https://doi.org/10.1002/2015WR017075>
- Marsh, P., & Woo, M.-K. (1984). Wetting front advance and freezing of meltwater within a snow cover: 1. Observations in the Canadian Arctic. *Water Resources Research*, 20(12), 1853–1864.
- McGrath, D., Colgan, W., Steffen, K., Lauffenburger, P., & Balog, J. (2011). Assessing the summer water budget of a moulin basin in the Sermeq Avannarleq ablation region, Greenland Ice Sheet. *Journal of Glaciology*, 57, 954–964.
- Miller, O. L., Solonon, D. K., Miège, C., Koenig, L., Forster, R. R., Montgomery, L. N., ... Brucker, L. (2017). Hydraulic conductivity of a firn aquifer system in southeast Greenland. *Frontiers in Earth Science*, 5, 38. <https://doi.org/10.3389/feart.2017.00038>
- Mitchell, A., Brown, G. H., & Fuge, R. (2001). Minor and trace element export from a glacierized alpine headwater catchment (Haut Glacier d'Arolla, Switzerland). *Hydrological Processes*, 15, 3499–3524. <https://doi.org/10.1002/hyp.1041>
- Moore, J. C., Pälli, A., Ludwig, F., Blatter, H., Jania, J., Gadek, B., ... Isaksson, E. (1999). High-resolution hydrothermal structure of Hansbreen, Spitsbergen, mapped by ground-penetrating radar. *Journal of Glaciology*, 45, 524–532. <https://doi.org/10.3198/1999JoG45-151-524-532>
- Moore, J. E. (2002). *Field hydrogeology: A guide for site investigations and report preparation*. New York, NY: Lewis.
- Müller, F., & Keeler, C. M. (1969). Errors in short term ablation measurement on melting ice surfaces. *Journal of Glaciology*, 8, 91–105.
- Munro, D. S. (1990). Comparison of melt energy computations and ablatometer measurements on melting ice and snow. *Arctic and Alpine Research*, 22, 153–162. <https://doi.org/10.2307/1551300>
- Munro, D. S. (2011). Delays of supraglacial runoff from differently defined microbasin areas on the Peyto glacier. *Hydrological Processes*, 25(19), 2983–2994. <https://doi.org/10.1002/hyp.8124>
- Nye, J. F. (1991). The rotting of temperate ice. *Journal of Crystal Growth*, 113, 465–476. [https://doi.org/10.1016/0022-0248\(91\)90081-F](https://doi.org/10.1016/0022-0248(91)90081-F)
- Oerlemans, J., Giesen, R. H., & van den Broeke, M. R. (2009). Retreating alpine glaciers: Increased melt rates due to accumulation of dust (Vadret da Morteratsch, Switzerland). *Journal of Glaciology*, 55(192), 729–736.
- Oke, T. R. (1987). *Boundary layer climates*. London, UK: Routledge.
- Paterson, W. S. B. (1994). *The physics of glaciers*. Pergamon, 480pp.
- Pavlova, P. A., Schmid, P., Bogdal, C., Steinlin, C., Jenk, T. M., & Schwikowski, M. (2014). Polychlorinated biphenyls in glaciers. 1. Deposition history from an alpine ice core. *Environmental Science & Technology*, 48, 7842–7848. <https://doi.org/10.1021/es5017922>
- Pellicciotti, F., Brock, B., Strasser, U., Burlando, P., Funk, M., & Corripio, J. (2005). An enhanced temperature-index glacier melt model including the shortwave radiation balance: Development and testing for Haut Glacier d'Arolla, Switzerland. *Journal of Glaciology*, 51, 573–587. <https://doi.org/10.3189/172756505781829124>
- Porter, P. R., Vatne, G., Ng, F., & Irvine-Fynn, T. D. (2010). Ice-marginal sediment delivery to the surface of a high-Arctic glacier: Austre Brøggerbreen, Svalbard. *Geografiska Annaler*, 92A(4), 437–449.

- Rassner, S. M. E., Anesio, A. M., Girdwood, S. E., Hell, K., Gokul, J. K., Whitworth, D. E., & Edwards, A. (2016). Can the bacterial community of a high arctic glacier surface escape viral control? *Frontiers in Microbiology*, 7, 956. <https://doi.org/10.3389/fmicb.2016.00956>
- Rennermalm, A. K., Smith, L. C., Chu, V., Box, J., Forster, R. R., Van den Broeke, M., ... Moustafa, S. E. (2013). Evidence of meltwater retention within the Greenland Ice Sheet. *The Cryosphere*, 7, 1433–1445.
- Reverter, F., Li, X., & Meijer, G. C. M. (2007). Liquid-level measurement system based on a remote grounded capacitive sensor. *Sensors and Actuators A*, 138, 1–8.
- Rippin, D. M., Pomfret, A., & King, N. (2015). High resolution mapping of supraglacial drainage pathways reveals link between micro-channel drainage density, surface roughness and surface reflectance. *Earth Surface Processes and Landforms*, 40(10), 1279–1290. <https://doi.org/10.1002/esp.3719>
- Ross, P. J. (1983). A water level sensor using a capacitance to frequency converter. *Journal of Physics E: Scientific Instruments*, 16, 827–828.
- Rudolph, J. V., Friedrich, K., & Germann, U. (2011). Relationship between radar-estimated precipitation and synoptic weather patterns in the European Alps. *Journal of Applied Meteorology and Climatology*, 50, 944–957. <https://doi.org/10.1175/2010JAMC2570.1>
- Rutter, N., Hodson, A., Irvine-Fynn, T., & Solås, M. K. (2011). Hydrology and hydrochemistry of a deglaciating high-Arctic catchment, Svalbard. *Journal of Hydrology*, 410(1–2), 39–50.
- Schneider, T. (1999). Water movement in the firn of Storglaciären, Sweden. *Journal of Glaciology*, 45(150), 286–294.
- Schuster, C. J. (2001). *Weathering crust processes on melting glacier ices (Alberta, Canada)*. (134pp) Wilfred Laurier University.
- Scott, D., Hood, E., & Nassry, M. (2010). In-stream uptake and retention of C, N and P in a supraglacial stream. *Annals of Glaciology*, 51(56), 80–86.
- Sharp, M., Richards, K. S., & Tranter, M. (1998). Introduction. In M. Sharp, K. S. Richards, & M. Tranter (Eds.), *Glacier hydrology and hydrochemistry* (pp. 1–14). Wiley.
- Shumskii, P. (1964). *Principles of structural glaciology: The petrography of fresh-water ice as a method of glaciological investigation*. (497pp). New York, NY: Dover.
- Singer, G. A., Fasching, C., Wilhelm, L., Niggemann, J., Steier, P., Dittmar, T., & Battin, T. J. (2012). Biogeochemically diverse organic matter in alpine glaciers and its downstream fate. *Nature Geoscience*, 5(10), 710–714. <https://doi.org/10.1038/ngeo1581>
- Smart, P., & Laidlaw, I. (1977). An evaluation of some fluorescent dyes for water tracing. *Water Resources Research*, 13, 15–33.
- Smith, L. C., Chu, V. W., Yang, K., Gleason, C. J., Pitcher, L. H., Rennermalm, A. K., ... Balog, J. (2015). Efficient meltwater drainage through supraglacial streams and rivers on the southwest Greenland Ice Sheet. *Proceedings of the National Academy of Sciences*, 112, 1001–1006. <https://doi.org/10.1073/pnas.1413024112>
- Smith, L. C., Yang, K., Pitcher, L. H., Overstreet, B. T., Chu, V. W., Rennermalm, A. K., ... Behar, A. E. (2017). Direct measurements of meltwater runoff on the Greenland Ice Sheet surface. *Proceedings of the National Academy of Sciences (early view)*, (10pp). <https://doi.org/10.1073/pnas.1707743114>
- St. Germain, S. L., & Moorman, B. J. (2016). The development of a pulsating supraglacial stream. *Annals of Glaciology*, 57, 31–38. <https://doi.org/10.1017/aog.2016.16>
- Stibal, M., Šabacká, M., & Žárský, J. (2012). Biological processes on glacier and ice sheet surfaces. *Nature Geoscience*, 5(11), 771–774.
- Stibal, M., Telling, J., Cook, J., Mak, K. M., Hodson, A., & Anesio, A. M. (2012). Environmental controls on microbial abundance and activity on the Greenland ice sheet: A multivariate analysis approach. *Microbial Ecology*, 63(1), 74–84.
- Takeuchi, N. (2002). Optical characteristics of cryoconite (surface dust) on glaciers: The relationship between light absorbency and the property of organic matter contained in the cryoconite. *Annals of Glaciology*, 34(1), 409–414.
- Theakstone, W. H., & Knudsen, N. T. (1981). Dye tracer tests of water movement at the glacier Austre Okstindbreen, Norway. *Norsk Geografisk Tidsskrift*, 35, 21–28. <https://doi.org/10.1080/00291958108621970>
- Wakahama, G. (1978). Observations of the melt-water permeation in the near-surface ice layers of the Mendenhall Glacier, South-east Alaska. *Materialy Glyatsiologicheskikh Issledovaniy. Khronika. Obsuzhdeniya*, 33, 175–178.
- Wakahama, G., Kuroiwa, D., Kobayashi, D., Tanuma, K., Endo, Y., Mizuno, Y., & Kobayashi, S. (1973). Observations of permeating water through a glacier body. *Low Temperature Science A*, 31, 217–219.
- van de Wal, R. S. W., Boot, W., van den Broeke, M. R., Smeets, C. J. P. P., Reijmer, C. H., Donker, J. J. A., & Oerlemans, J. (2008). Large and rapid melt-induced velocity changes in the ablation zone of the Greenland Ice Sheet. *Science*, 321, 111–113. <https://doi.org/10.1126/science.1158540>
- van de Wal, R. S. W., Greuell, W., van den Broeke, M. R., Reijmer, C. H., & Oerlemans, J. (2005). Surface mass-balance observations and automatic weather station data along a transect near Kangerlussuaq, West Greenland. *Annals of Glaciology*, 42, 311–316. <https://doi.org/10.3189/172756405781812529>
- Wainstein, P., Moorman, B., & Whitehead, K. (2014). Glacial conditions that contribute to the regeneration of fountain glacier proglacial icing, Bylot Island, Canada. *Hydrological Processes*, 28, 2749–2760. <https://doi.org/10.1002/hyp.9787>
- Whitehead, K., Moorman, B. J., & Hugenholtz, C. H. (2013). Brief communication: Low-cost, on-demand aerial photogrammetry for glaciological measurement. *The Cryosphere*, 7, 1879–1884. <https://doi.org/10.5194/tc-7-1879-2013>
- Whitehead, K., Moorman, B. J., & Wainstein, P. (2014). Measuring daily surface elevation and velocity variations across a polythermal arctic glacier using ground-based photogrammetry. *Journal of Glaciology*, 60, 1208–1220. <https://doi.org/10.3189/2014JoG14J080>
- Wilhelm, L., Singer, G. A., Fasching, C., Battin, T. J., & Besemer, K. (2013). Microbial biodiversity in glacier-fed streams. *ISME Journal*, 7(8), 1651–1660. <https://doi.org/10.1038/ismej.2013.44>
- Willis, I. C., Arnold, N. S., & Brock, B. W. (2002). Effect of snowpack removal on energy balance, melt and runoff in a small supraglacial catchment. *Hydrological Processes*, 16, 2721–2749. <https://doi.org/10.1002/hyp.1067>
- Wilner, L. B. (1960). Variable capacitance liquid level sensor. *Review of Scientific Instruments*, 31, 501–507.
- Yang, K., Karlstrom, L., Smith, L. C., & Li, M. (2016). Automated high-resolution satellite image registration using supraglacial rivers on the Greenland Ice Sheet. *IEEE Journal of Selected Topics in Applied Earth Observations and Remote Sensing*, 10(3), 845–856.
- Yang, K., & Smith, L. C. (2013). Supraglacial streams on the Greenland Ice Sheet delineated from combined spectral-shape information in high-resolution satellite imagery. *IEEE Geoscience and Remote Sensing Letters*, 10, 801–805.
- Younger, P. L. (2009). *Groundwater in the environment: An introduction*. Wiley.
- Zeng, Q., Cao, M., Feng, X., Liang, F., Chen, X., & Sheng, W. (1984). A study of spectral reflection characteristics for snow, ice and water in the north of China. *Hydrological Applications of Remote Sensing and Remote Data Transmission*, 145, 451–462.

How to cite this article: Stevens IT, Irvine-Fynn TDL, Porter PR, et al. Near-surface hydraulic conductivity of northern hemisphere glaciers. *Hydrological Processes*. 2018;32:850–865. <https://doi.org/10.1002/hyp.11439>